ULTRAFINE GRAINED MATERIALS

Multiscale modeling of back-stress evolution in equal-channel angular pressing: from one pass to multiple passes

**Enze Chen · Laurent Duchêne ·
Anne Marie Habraken · Bert Verlinden**

Abstract Fine-grained materials produced by equal-channel angular pressing (ECAP) exhibit kinematic hardening due to the existence of a back-stress. This article presents a new dislocation-based model, which is able to describe the tension/compression asymmetry of the ECAP processed commercial purity aluminum. By introducing strain relaxation, and relating the back-stress to the inhomogeneous dislocation density distribution in cell walls and in cell interiors, the model can accurately predict the evolution of the dislocation densities, the cell size, and the back-stress. Compared to the other back-stress models, it takes into account the microstructure evolution and gives a better prediction.

Introduction

It has been found that materials, which are processed by equal-channel angular pressing (ECAP) exhibit significant kinematic hardening during mechanical tests, e.g., the tension/compression asymmetry [1]. This phenomenon is

E. Chen (✉) · B. Verlinden
Department of Metallurgy and Materials Engineering,
Katholieke Universiteit Leuven, Kasteelpark Arenberg 44,
3001 Heverlee, Belgium
e-mail: enze.chen@mtm.kuleuven.be

B. Verlinden
e-mail: bert.verlinden@mtm.kuleuven.be

L. Duchêne · A. M. Habraken
FNRS Fonds de la Recherche Scientifique, University of Liège,
ARGENCO, Chemin des Chevreuils 1, 4000 Liège, Belgium
e-mail: l.duchene@ulg.ac.be

A. M. Habraken
e-mail: Anne.Habraken@ulg.ac.be

due to the existence of back-stresses, induced by the inhomogeneous dislocation density distribution in the developed dislocation structures, resulting from the severe plastic deformation.

Mughrabi [2] modeled these dislocation microstructures as being composed of a soft phase, *cell interiors* or channels, with a low dislocation density ($\rho_c < 10^{14}$ m^{-2}, often mobile dislocations) and a hard phase, *cell walls*, with a high dislocation density ($\rho_w > 10^{15}$ m^{-2}, often edge dipoles).

In our previous work [3], the back-stresses in ECAP processed commercial purity aluminum were calculated using a phenomenological mixed hardening model from Teodosiu and Hu [4, 5] and using a new physical model, which is based on the Estrin–Tóth's work [6] combined with the intragranular back-stress from Sauzay [7]. It has been shown that the new physical model was much better than the phenomenological one in predicting the appropriate back-stress level of Al after one ECAP pass.

In the present article, this dislocation-based model was modified and extended to describe the back-stress evolution during further ECAP processing, making it able to describe *strain path change* deformation. This modified model will be used to study both the evolution of the microstructure and back-stress behavior of commercial purity aluminum during multiple pass ECAP processing following route C.

Definition of the back-stress

It is definitely necessary to define the physical meaning of the back-stress first, since the term *back-stress* has been widely used in different length-scales, making its meaning rather confused.

From a macroscopic view, this term is normally used when the same material exhibits different yield strength in a sequential deformation such as the Bauchinger deformation and the orthogonal deformation. The back-stress is defined as a function of the difference of the yielding stress. Furthermore, the macroscopic back-stress can be interpreted as the translation of the yield locus in the stress space in many kinematic hardening models. The existence of this stress is considered as the result of the anisotropic hardening.

On the other hand, from a microscopic view, the term back-stress can also refer to the long-range internal stress. For the materials containing strong particles, the back-stress is essentially the Orowan stress between the dislocations and the particles. It will help the dislocations to move backward easier than to move forward because the particles behaves like obstacles to the dislocations. For dislocation-cell-forming materials, the back-stress is an unavoidable consequence of the compatibility requirements in the presence of a heterogeneous dislocation distribution in the cell wall and the cell interior [2].

In this article, the macroscopic back-stress is defined as the average of the microscopic internal stress resulting from the different dislocation density in cell wall and cell interior. Under this assumption, the predicted back-stress by the current model is able to be compared with the macroscopic back-stress measured from the experiments.

Modeling approach

Two mechanisms are taken into account to describe the anisotropic softening/hardening behavior of material under large strain and strain path change condition: the textural evolution and the evolution of the microstructure.

Crystal plasticity framework

The Taylor–Bishop–Hill theory is used as a framework to develop the current model. As often [8, 9], the elastic strain is neglected. Starting from the initial texture, the Taylor model is able to predict both the slip activity in crystals and the updated texture for any strain path.

Consider an arbitrary velocity gradient tensor l_{ij} that is imposed on a crystal. A kinematic equation relates this tensor with the slip rate $\dot{\gamma}_s$ of the N active slip systems with index s:

$$l_{ij} = \sum_{s=1}^{N} b_i^s m_j^s \dot{\gamma}_s + \dot{\Omega}_{ij}, \tag{1}$$

where the unit vector b^s represents the slip direction of slip system s and the unit vector m^s is normal to the slip plane of slip system s, and $\dot{\Omega}_{ij}$ is the lattice rotation rate.

Taylor himself [10] assumed that, among all possible solutions for Eq. 1, only those consuming the lowest energy are the best solutions. Mathematically, his assumption describes a linear constraint optimization problem, which can be solved by the simplex method [6] or the interior point method:

$$\text{minimize: } P = \sum_{s=1}^{N} \tau_s^c |\dot{\gamma}_s|$$

$$\text{subject to: } d_{ij} = \sum_{s=1}^{N} \frac{1}{2} \left(b_i^s m_j^s + m_i^s b_j^s \right) \dot{\gamma}_s \tag{2}$$

in which the internally dissipated frictional work rate P is treated as the objective function, τ_s is the critical resolved shear stress (CRSS) of slip system s, and the strain rate tensor d_{ij} is the symmetric part of the velocity gradient tensor l_{ij}.

Once the optimized solution $\dot{\gamma}_s$ is known, the lattice rotation rate can be calculated as the difference between the plastic spin w_{ij} and the skew-symmetric part of the velocity gradient:

$$\dot{\Omega}_{ij} = w_{ij} - \sum_{s=1}^{N} \frac{1}{2} \left(b_i^s m_j^s - m_i^s b_j^s \right) \dot{\gamma}_s. \tag{3}$$

This tensor $\dot{\Omega}_{ij}$ makes it possible to update the orientation of each grain, which determines the evolved texture after each deformation step.

For simplicity, the full-constraint Taylor model is adopted. It assumes that the local velocity gradient imposed on a grain is equal to the macroscopic velocity gradient.

Evolution of the dislocation cell structure

It is well known that, starting from the work hardening in stage III, the dislocations develop and self organize in cells, creating cell walls with high dislocation density and cell interiors with low density [2]. In this respect, many composite models have been developed in the past. Among them the Estrin–Tóth model [6] is valid for all hardening stages at large strain and has been frequently applied to model ECAP processing. It is introduced into the current modeling framework to describe the evolution of the dislocation cells. However, two parts of the Estrin–Tóth model are modified. First, the assumption of identical strain rate in cell walls and cell interiors is relaxed. Second, the strain rate sensitivity is neglected.

Estrin and Tóth assumed that the strain rate is identical both in cell walls and in cell interiors. However, according to the experimental in situ TEM observations of Tabata et al. [11, 12], the dislocations glide much faster in the middle of the cells than near the walls and the plastic glide in the walls is much reduced. This evidence implies the need to relax the strong assumption of Estrin and Tóth. A

factor ϑ is defined as the ratio between the slip rate in the cell wall and the slip rate in the cell interior:

$$\vartheta = \dot{\gamma}_w / \dot{\gamma}_c. \tag{4}$$

This factor results in the modification of the strain rate equation:

$$\dot{\gamma}_w = \frac{2}{1+\vartheta}\dot{\gamma}^r, \\ \dot{\gamma}_c = \frac{2\vartheta}{1+\vartheta}\dot{\gamma}^r, \tag{5}$$

in which the equivalent strain rate of the cell structure $\dot{\gamma}^r$ is a function of the slip rates of the N active slip systems of the studied crystal:

$$\dot{\gamma}^r = \sum_{s=1}^{N} |\dot{\gamma}_s|. \tag{6}$$

The introduction of this relaxation does not change the strain compatibility:

Original assumption: $\dot{\gamma}_w + \dot{\gamma}_c = \dot{\gamma}^r + \dot{\gamma}^r = 2\dot{\gamma}^r,$

Relaxed assumption: $\dot{\gamma}_w + \dot{\gamma}_c = \frac{2}{1+\vartheta}\dot{\gamma}^r + \frac{2\vartheta}{1+\vartheta}\dot{\gamma}^r = 2\dot{\gamma}^r.$
$$\tag{7}$$

The most interesting idea of Estrin–Tóth's model is that it introduces an evolution law of the volume fraction of cell walls f based on the work of Müller et al. [13]:

$$f = f_\infty + (f_0 - f_\infty)\exp\left(\frac{-\gamma^r}{\tilde{\gamma}^r}\right), \tag{8}$$

where f_0 is the initial value of the volume fraction of cell walls, f_∞ is its saturation value at large strains. The quantity $\tilde{\gamma}^r$ describes the variation rate of f with resolved shear strain γ^r. This volume fraction allows not only calculating the cell size d by:

$$d = \frac{K}{\sqrt{f\rho_w + (1-f)\rho_c}}, \tag{9}$$

but also averaging the critical resolved shear stress

$$\tau = f\tau_w + (1-f)\tau_c \\ = f\alpha Gb\sqrt{\rho_w} + (1-f)\alpha Gb\sqrt{\rho_c}, \tag{10}$$

in which K and α are material constants, G the shear modulus, and b the Burgers vector.

The evolution law of the dislocation density both in the cell wall ρ_w and the cell interior ρ_c can be described by the two following equations:

$$\dot{\rho}_c = \alpha^* \frac{1}{\sqrt{3}} \frac{\sqrt{\rho_w}}{b} \dot{\gamma}_w - \beta^* \frac{6\dot{\gamma}_c}{bd(1-f)^{1/3}} - k_0 \dot{\gamma}_c \rho_c, \\ \dot{\rho}_w = \frac{\sqrt{3}\beta^* \dot{\gamma}_c (1-f)\sqrt{\rho_w}}{fb} + \frac{6\beta^* \dot{\gamma}_c (1-f)^{2/3}}{bdf} - k_0 \dot{\gamma}_w \rho_w, \tag{11}$$

where α^* and β^* are geometrical parameters. Both these two evolution equations contain three terms, which contributes from different dislocation mechanisms. The first terms describe the rate of generation of dislocations generated by Frank–Read sources at the interface between the cell wall and the cell interior. The second one comes from the dislocation motion, moving from cell interior to cell wall or from cell wall to cell interior. The last part is given by the mutual annihilation of dislocations with opposite sign. More information about the Estrin–Tóth model can be found in [6].

Evolution of the back-stress

Reconsidering the Sauzay's intragranular back-stress model

In the current authors' previous work [3], the long-range internal stress or back-stress was calculated using the intragranular back-stress model from Sauzay [7]. As usual, the plasticity problem of a two-phase cell structure was treated as an inclusion problem. Sauzay proposed to introduce a so-called plastic accommodation factor F_{accom}, which has been used in the polycrystalline self-consistent model [14]. In this way, the back-stress is limited by reducing the incompatibilities between cell walls and cell interiors. The factor F_{accom} makes it possible to compute the 3D back-stress tensor x_{ij}:

$$x_{ij} = -\frac{f}{1-f}G(1-\beta)F_{accom}\sum_{s=1}^{N}\left(b_i^s m_j^s + m_i^s n_j^s\right)\gamma_s^p, \tag{12}$$

in which β is a scalar function of the Poisson coefficient and γ_s^p is the total plastic slip of slip system s. This equation succeeded in predicting the back-stress of commercial purity aluminum processed by one ECAP pass [3]. However, this is no longer the case for a *strain path change* deformation. The reason for this can be understood as follows.

Investigate the derivative of x_{ij} with respect to time:

$$\overset{\circ}{x_{ij}} \cong -\frac{f}{1-f}G(1-\beta)F_{accom}\sum_{s=1}^{N}\left(b_i^s m_j^s + m_i^s n_j^s\right)\gamma_s^p \\ = -\frac{f}{1-f}G(1-\beta)F_{accom}d_{ij}, \tag{13}$$

in which d_{ij} is the imposed strain rate. This equation implies the proportionality between the derivative of the back-stress and the strain rate: $\overset{\circ}{x_{ij}} \propto d_{ij}$. Now assume that an annealed crystal without any initial back-stress is loaded by a forward and then a reverse Bauschinger deformation. According to Eq. 13, the reverse deformation more or less ensures the opposite slip direction of slip systems. If the equivalent strain of the reverse deformation is identical to the forward

one, it will result in the back-stress decreasing to the initial value or near its original state before the deformation. In other words, there exists no back-stress anymore in this crystal! This result is totally in contrast with the experimental evidence: a dissolution-reconstruction mechanism is active during the first stage of the subsequent loading path, accompanying a transient softening of the material [15]. However, it is impossible that the back-stresses totally vanish after a Bauschinger test. This discussion proves that Sauzay's intragranular back-stress model is not valid for strain path change deformation.

A dislocation-based intragranular back-stress model

The invalidation of the Sauzay's model for the strain path change deformation is due to the fact that the dislocation rearrangements are neglected. These rearrangements can be taken into account by adding a recovery part in the right hand side of Eq. 13, which makes it very similar to the Armstrong and Frederick's nonlinear kinematic hardening law [16]:

$$\overset{\circ}{x}_{ij} = k_r k_d d_{ij} - k_r x_{ij} \dot{\bar{\varepsilon}}_{eq}, \tag{14}$$

in which k_r is a factor controlling the back-stress recovery rate due to the dislocation rearrangement and k_d is a factor related to the dislocation density. Note that the sign of the back-stress in Eq. 14 is opposite to the one in Sauzay's model. k_d is defined as a function of the dislocation density in cell walls and the dislocation density in cell interiors:

$$k_d = \frac{f}{1-f} \alpha G b \left(\sqrt{\rho_w} - \sqrt{\rho_c} \right). \tag{15}$$

Combining Eqs. 14 and 15, the back-stress evolution law becomes:

$$\overset{\circ}{x}_{ij} = k_r \frac{f}{1-f} \alpha G b \left(\sqrt{\rho_w} - \sqrt{\rho_c} \right) d_{ij} - k_r x_{ij} \dot{\bar{\varepsilon}}_{eq}, \tag{16}$$

in which the term $\frac{f}{1-f}$ represents the volume ratio between the cell wall and the cell interior. This equation implies that the long-range internal back-stress is induced from the dislocation density difference. The contribution comes from the different critical resolved shear stresses in the cell wall and in the cell interior. This equation coincides with the phenomenological back-stress evolution law in the Teodosiu–Hu model [4, 5]. However, compared to the Teodosiu–Hu model, the current back-stress law has a clearer physical meaning.

Implementation detail

The three parts mentioned above, textural evolution, dislocation development, and corresponding long-ranged internal stress make up a complete dislocation-based model

for strain path change deformation. A yielding criterion is proposed for this model:

$$Y_{ij} - \sqrt{(\sigma_{ij} - x_{ij})(\sigma_{ij} - x_{ij})} = 0, \tag{17}$$

in which Y_{ij} is the isotropic hardening term calculated by the Taylor model based on the predicted CRSS from Eq. 10, σ_{ij} is the effective Cauchy stress imposed on the material.

The whole model is implemented using Intel Visual Fortran. The IMSL (International Mathematics and Statistics Library) Fortran numerical library is used to solve two mathematical problems. On one hand, the subroutine DLPRS (revised simplex method) is called to solve the linear programming problem in the Taylor single crystal plasticity model (Eq. 2). On the other hand, the subroutine IVPAG (Adams–Moulton's method) is called to solve the initial-value problem for the dislocation evolution equations (Eq. 11).

The current model needs to identify several material parameters: ϑ, α^*, β^*, k_0, and k_r.

Application of the model: ECAP processing of aluminum (route C)

Before presenting how to use the current model to simulate the ECAP processing, it is necessary to explain how the experimental macroscopic back-stresses of post-ECAP aluminum are obtained.

Experimental

The used ECAP die (see Fig. 1) is mounted on a hydraulic press with a maximum force up to 110 kN. The channel angle Φ is 90° and the additional angle Ψ, which represents the arc of the curvature where the two parts of the channel intersect, is 0°. According to the work of Iwahashi et al. [17], the imposed shear strain γ after each pass is equal to 2 and the equivalent strain is around 1.15. The global reference frame ED–ND–TD is established by right-handed convention.

The experimental material was cut from a hot-rolled plate of commercial purity aluminum AA1050. Its initial mean grain size was about 25–33 μm, measured by electron backscattered diffraction (EBSD). The texture was measured by a Siemens D500 goniometer and discretized into a representative set of 2,000 orientations.

In this article, only four ECAP passes at room temperature of route C (180° rotation between each pass) are investigated. The punch pushed the sample through the die at a constant speed of 10 mm/min. MoS$_2$ lubricant was used to reduce the friction between the sample and the
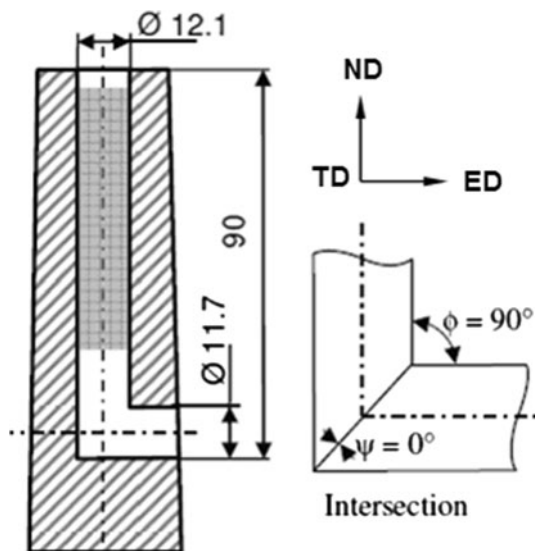
Fig. 1 A schematic of the ECAP die and the macroscopic reference frame

channel surface and to avoid that the samples get stuck in the die.

The tensile specimens and the compression specimens were machined from the homogenous part of the ECAP processed cylindrical samples. The two kinds of tests were performed separately on a mechanical test machine INSTRON 4505. The yielding strength both of the tensile tests and the compression tests were determined by using the offset method, which corresponds to a small offset strain of 0.002. The results are shown in Fig. 2.

The macroscopic back-stress is defined as a function of the yielding strength of the tensile test $\sigma_{\text{tensile}}^{\text{y}}$ and the one of the compression test $\sigma_{\text{compression}}^{\text{y}}$:

Table 1 The measured back-stress along ED of the ECAP processed AA1050 sample

ECAP pass	Pass 1	Pass 2	Pass 3	Pass 4
Back-stress (MPa)	29.5	33.0	39.5	47.5

$$x_{\text{ED}} = \frac{1}{2}\left(\sigma_{\text{tensile}}^{\text{y}} - \sigma_{\text{compression}}^{\text{y}}\right), \tag{18}$$

in which x_{ED} means that the measured back-stress component parallel with the extrusion direction of the ECAP die. The calculated back-stress is shown in Table 1.

Simulation details

The initial material is assumed to be homogeneous. According to this assumption, a hypothetical cubic material element normal to the shear plane is inserted into the ECAP die and deformed on the shear plane (see Fig. 3). In odd passes, the shape of the element is changed into a parallelogram. For the subsequent passes, instead of simulating the rotation of the element and inserting it into the die again, the element is assumed to be pressed into an infinite-length continuous ECAP die, which contains parallel shear planes (Fig. 3). It is proved that this procedure is totally identical to the discontinuous ECAP processing using route C [18]. In the even passes, the parallelogram is sheared back to a cubic element.

A local frame is established, so that its axis 1 is normal to the shear plane and its axis 2 is parallel to the shear plane. This local frame retains its orientation through the whole processing. The local velocity gradients L_{ij} are reversed after each pass (simulated by 100 steps):
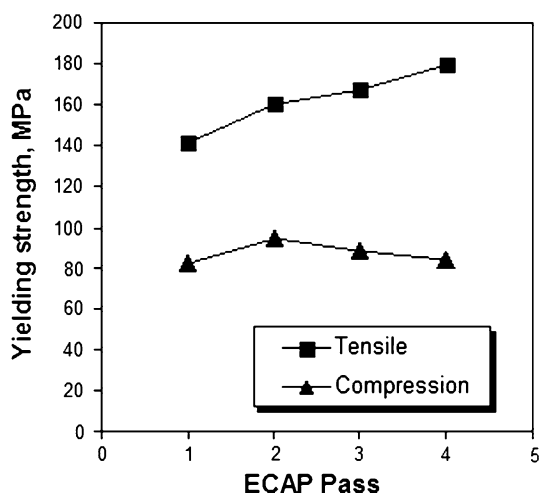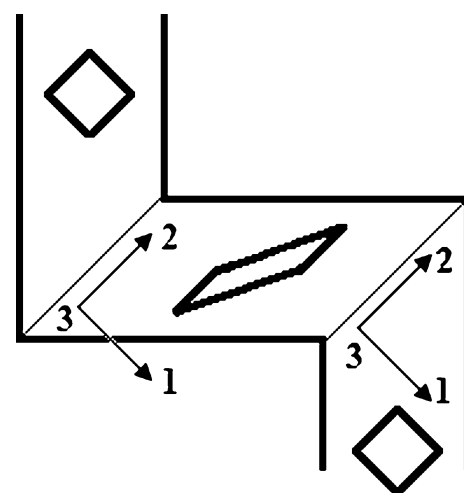

Fig. 2 The yielding strength of the ECAP processed commercial purity aluminum AA1050 determined from tensile tests and from compression tests

Fig. 3 A schematic of the simulation procedure. A cubic element is sheared into a parallelogram in odd passes and is sheared back into cubic shape in even passes. The local reference fixed on the shear plane is retained during the whole procedure

$$L_{ij}^{\text{odd pass}} = \begin{bmatrix} 0 & 0 & 0 \\ 2 & 0 & 0 \\ 0 & 0 & 0 \end{bmatrix} \dot{\gamma} \text{ and } L_{ij}^{\text{even pass}} = \begin{bmatrix} 0 & 0 & 0 \\ -2 & 0 & 0 \\ 0 & 0 & 0 \end{bmatrix} \dot{\gamma}. \tag{19}$$

The 2,000 crystalline orientations from the texture measurement are expressed into this local frame and submitted to the shearing deformation. Their orientation will evolve during the deformation.

The back-stress tensor should be rotated to the macroscopic reference frame ED–TD–ND in order to get the back-stress value along ED. The rotation is different for odd passes and for even passes. Using the Euler's angle notation $(\varphi_1, \phi, \varphi_2)$, the rotation is (45,0,0) for every odd pass from 1–2–3 to ED–ND–TD, and (−45,180,0) for every even pass from 1–2–3 to ED–ND–TD.

Numerical results

Most material parameters of the current model are the same as in previous work [3]. Some of them (G, b) are known material parameters; others such as f_0, f_∞ are taken from reference [19]. The initial value for the dislocation densities in the cell walls and the cell interiors were 10^{13} and 10^{12} m^{-2}, respectively. The three parameters, α^*, β^*, and k_0 have the same value as in reference [19], and finally the new parameters such as ϑ and k_r are adjusted to obtain a best fit. All the parameters used in the current model are listed in Table 2.

The evolution of the dislocation density is shown in Fig. 4. The rate of the immobilization of the dislocations is much higher in the cell walls than in the cell interiors. At the end of the ECAP pass 4, the dislocation density in the cell walls reaches 7.638×10^{16} m^{-2}. This is very close to the experimental result from Müller et al. [13]. Instead, the
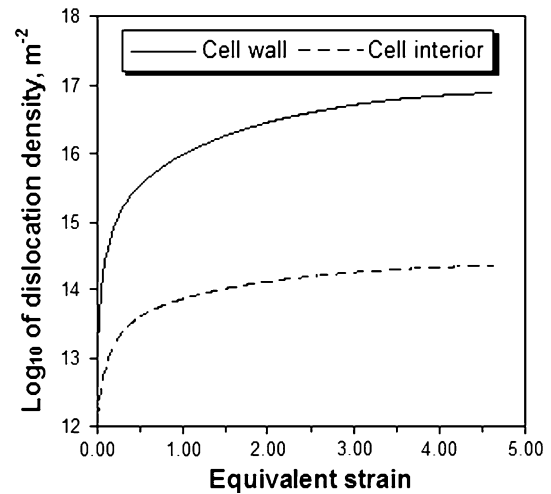

Fig. 4 The evolution of the dislocation density in cell walls and in cell interiors

dislocation density in the cell interior is still lower than 10^{14} m^{-2}.

The increase of the average dislocation density results in a decrease of the cell size. The cell size in the aluminum is close to 2.5 μm after one pass and decreases to 1.4 μm after four passes (Fig. 5). Compared to the EBSD measurement of previous work [20], the calculated cell size evolution is acceptable.

The predicted back-stress along the axis of the ECAP samples is shown in Fig. 6. The model predicts that the back-stress increases very fast in the first ECAP pass, and then reaches saturation and increases more slowly. The damping after each pass, during which the back-stress suddenly decreases below zero is due to the rotation of the
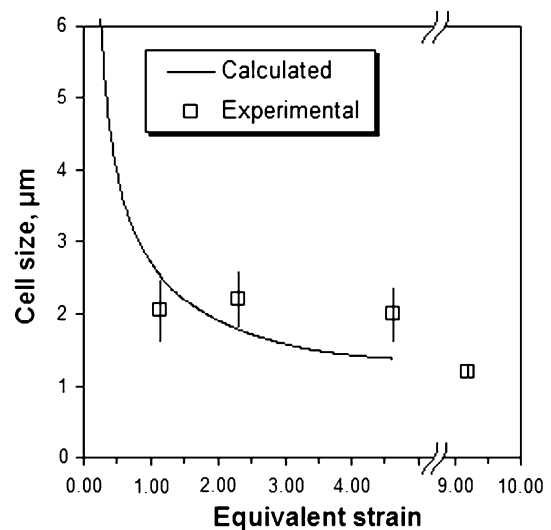
Table 2 Survey of the material parameters, used in the current model

Material parameters	Value
$\rho_w^{t=0}$ (m^{-2})	10^{13}
$\rho_c^{t=0}$ (m^{-2})	10^{12}
f_0	0.25
f_∞	0.06
α	0.35
G (GPa)	26.3
b (m)	2.86×10^{-10}
K	100
α^*	0.0024
β^*	0.0054
k_0	3.22
ϑ	0.52
k_r	10

Fig. 5 The evolution of the average cell size with respect to the equivalent strain; open symbols indicate subgrain sizes measured by EBSD
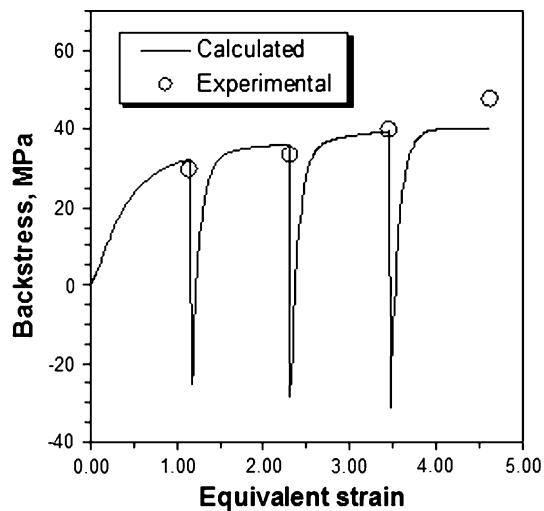
Fig. 6 The calculated back-stress evolution curve compared with the experimental measurements

sample before reinserting for the next ECAP processing. Its fast development implies the deconstruction of the former dislocation structures and rearrangement of the dislocations. The predicted back-stress after pass 1, pass 2, and pass 3 is very close to the experimental result. However, the difference after pass 4 is relatively larger.

The effective stress σ_{ij} is another important aspect, which needs comparison with the experimental results. In Fig. 7, the effective stress along the axis of ECAP samples is increasing very fast in odd passes and keeps the strength relatively constant during the even passes. At the end of each pass, the effective stress can be considered as the yielding strength in a tensile test that would be performed
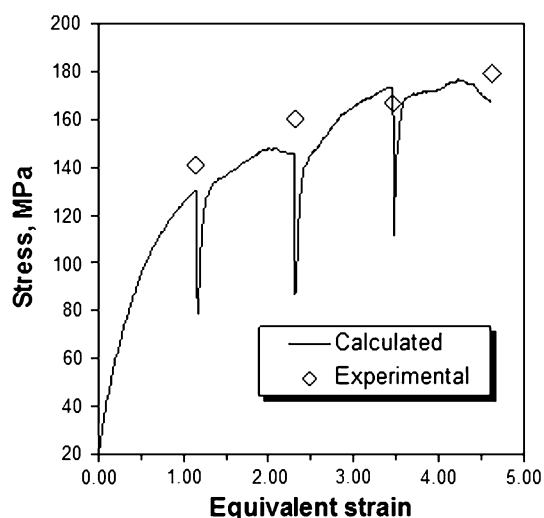
on these samples. The difference between the calculated results and the experimental results are acceptable.

Based on those results, it is believed that the current model captures very well the back-stress evolution of the ECAP processing of aluminum using route C.

Discussion

The strain relaxation in a cell-and-wall structure

As mentioned above, the Estrin–Tóth model assumed that the strain rate is identical both in the cell wall and the cell interior. On the other hand, Kröner [21] and Lemoine et al. [22] treat the cell wall as a thermoelastic material, which means there is no plastic slip in the cell wall and the plastic strain is all undertaken by the cell interior. According to the authors' understanding, these two kinds of treatments represent two extreme situations. Let R be defined as the dislocation density ratio between the cell wall and the cell interior. Figure 8 shows the large difference between the predicted R when different relaxation ratio $\vartheta = \dot{\gamma}_w/\dot{\gamma}_c$ is set. It is believed that the homogeneous strain assumption ($\vartheta = 1$) from the Estrin–Tóth model describes the lower bound, while these thermoelastic models ($\vartheta \to 0$) represents the upper bound of the dislocation evolution. A low-relaxation factor ϑ means lower dislocation mobility in cell walls, resulting in less chance of annihilation of the dislocations in cell walls and more mobile dislocations from cell interiors will stop at the cell walls. With the help of this factor, the current model with $\vartheta = 0.52$, locates between these two bounds, reflecting a dislocation evolution that is probably closer to the reality.
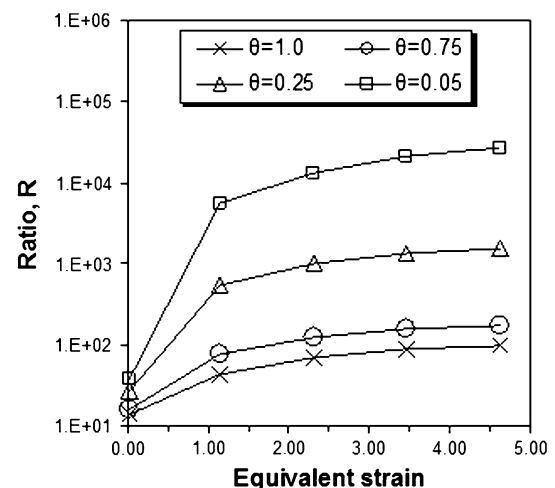

Fig. 7 The predicted effective stress during the ECAP processing compared to the yielding strength of the ECAP processed aluminum AA1050

Fig. 8 The influence of the strain relaxation factor ϑ on the dislocation density ratio R. R is defined as the dislocation density ratio between in the cell wall and in the cell interior

The behavior of the current dislocation-based back-stress law

According to the literature, there are at least three types of back-stress laws to predict this long-ranged internal stress. The first type is based on inclusion models. They are inspired by Eshelby's idea of treating the cell interior as the inclusion of the cell wall matrix [23, 24]. This type of laws is usually close to the thermoelastic theory, which always overestimates the back-stress. In order to overcome this drawback, Sauzay introduced a so-called plastic accommodation factor based on the ideas of self-consistent models. It works fine for monotonic deformation. The second type of models is more phenomenological and need adjustable parameters. Among them, both the model from Armstrong and Frederick [16] and the model from Chaboche and Rousselier [25] are very classic and famous. The development of this type of models was achieved by the work of Teodosiu and Hu. The adjustable parameters are related to the change of the dislocation sheets arrangements. The third type of models was first proposed by Mughrabi. The back-stress is assumed to be induced from the different strength of cell walls and cell interiors. Recently Feaugas and Gaudin ascribed the back-stress to the different dislocation density between cell walls and cell interiors [26].

The present dislocation-based model is a hybrid model. It adopts the expression from the phenomenological model to calculate the 3D back-stress and the influence from the strain path change. It takes the evolved dislocation densities into account to describe the increased influence from the back-stress source. Finally, the strain relaxation is considered to account for the strain heterogeneity in the cell structure.

In the current authors' previous work [3, 27], the model from Teodosiu and Hu, the model from Evers et al. [28, 29], and the model from Sauzay have been used to calculate the back-stress evolution during the EACP processing (see Fig. 9).

The first two models cannot predict the back-stress at an appropriate level, even not the correct evolution. Sauzay's model is relatively better and is able to predict values very close to the experimental ones. However, it is only suitable for monotonic deformation (only one ECAP pass). The current model is the best model to predict the back-stress after the first three passes. The experimental dots and the predicted ones are almost overlapping with each other.

The difference for the fourth pass is considered as the result of a relatively inaccurate texture evolution prediction and the fact that the difference between slip systems has been neglected. First, according to reference [18], prediction of the texture evolution in route C has proven to be quite challenging. Many aspects such as grain–grain
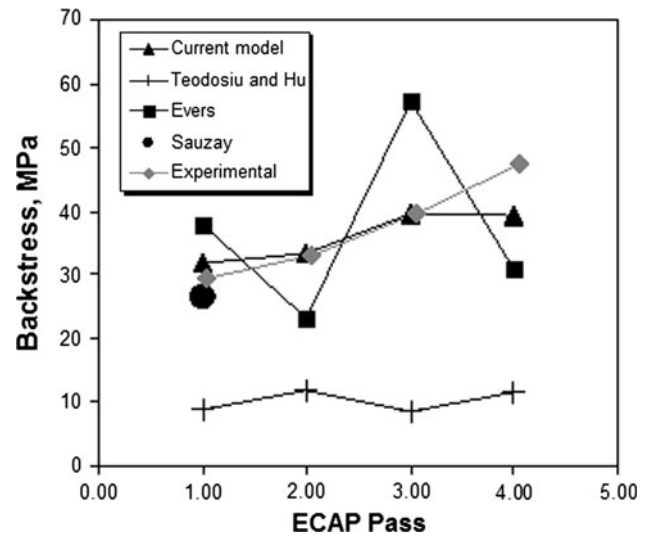

Fig. 9 The calculated back-stress from different models, compared with the experimental measurements

interaction, inhomogeneous deformation, grain hardening, grain substructure evolution, and imperfect reversal will influence the texture evolution. Any small mistake in the modeling assumption can lead to a bad texture prediction. Second, the slip systems do not evolve equally due to the grain orientation and latent hardening. The strong assumption of identical critical resolved shear stress not only induces the solution ambiguity of the FC-Taylor model, but it significantly influences the slip rate and underestimates the anisotropic evolution of the slip systems. These two problems need to be investigated further.

Conclusion

In this article, a dislocation-based model, with the idealization of a cell into a cell wall and a cell interior, was developed to simulate the ECAP processing following route C and to capture the evolution of the back-stress. By comparing the prediction with the experimental work, it has been proved the following.

1. This model accurately predicts the evolution of the dislocation density in the cell structure. It gives very realistic values of the cell size, comparable to the results of EBSD measurements.
2. The strain relaxation is introduced to describe the strain heterogeneity of a cell structure, making the model closer to capture the reality.
3. The current dislocation-based back-stress model adopts many advantages from the other back-stress models. It is shown that it can give an accurate back-stress evolution at least for the first three ECAP passes of route C.

References

1. Valiev RZ, Langdon TG (2006) Prog Mater Sci 51:881
2. Mughrabi H (1987) Phys Status Solidi A 104:107
3. Chen E, Duchêne L, Habraken AM, Verlinden B (in press) Rev Adv Mater Sci
4. Teodosiu C, Hu Z (1998) In: Proceedings of the 19th Risø international symposium on modelling of structures and mechanics of materials, p 149
5. Haddadi H, Bouvier S, Banu M, Maier C, Teodosiu C (2006) Int J Plast 22:2226
6. Estrin Y, Tóth LS, Molinari A, Brechet Y (1998) Acta Mater 46:5509
7. Sauzay M (2008) Int J Plast 24:727
8. Van Houtte P (1988) Textures Microstruct 8–9:313
9. Van Houtte P, Kanjarla AK, Van Bael A, Seefeldt M, Delannay L (2006) Eur J Mech A Solids 25:634
10. Taylor GI (1937) J Inst Met 62:307
11. Tabata T, Yamanaka S, Fujita H (1978) Acta Metall 26:405
12. Tabata T, Fujita H, Hiraoka M-A, Miyake S (1982) Philos Mag A 46:801
13. Müller M, Zehetbauer M, Borbély A, Ungár T (1996) Scr Mater 35:1461
14. Berveiller M, Zaoui A (1979) J Mech Phys Solids 26:325
15. Rauch EF, Schmitt JH (1989) Mater Sci Eng A 113:441
16. Armstrong PJ, Frederick CO (1966) Berkeley Nuclear Laboratories, GEGB report RD/B/N731
17. Iwahashi Y, Wang J, Horita Z, Nemoto M, Langdon TG (1996) Scr Mater 35:143
18. Beyerlein IJ, Tóth LS (2009) Prog Mater Sci 54:427
19. Baik SC, Estrin Y, Kim HS, Hellmig RJ (2003) Mater Sci Eng A 351:86
20. Poortmans S, Duchêne L, Habraken AM, Verlinden B (2009) Acta Mater 57:1821
21. Kröner E (1961) Acta Metall 9:155
22. Lemoine X, Muller D, Berveiller M (1994) Mater Sci Forum 157–162:1821
23. Eshelby JD (1959) Proc R Soc A 252:561
24. Pedersen OB (1990) Acta Metall Mater 38(7):1221
25. Chaboche JL, Rousselier G (1983) ASME J Press Vessel Technol 105:153
26. Feaugas X, Gaudin C (2001) Mater Sci Eng 309–310:382
27. Duchêne L, Geers MGD, Brekelmans WAM, Chen E, Verlinden B, Habraken AM (2009) Mater Process Text 671. doi:10.1002/9780470444191.ch76
28. Evers LP, Brekelmans WAM, Geers MGD (2004) J Mech Phys Solids 52:2379
29. Evers LP, Brekelmans WAM, Geers MGD (2004) Int J Solids Struct 41:5209